Accepted draft, April 30, 2014

JOURNAL OF GEOPHYSICAL RESEARCH, VOL. ???, XXXX, DOI:10.1029/,

Observed holiday aerosol reduction and temperature cooling over East Asia

Dao-Yi Gong,[1] Wenshan Wang,[2] Yun Qian,[3] Wenbing Bai,[4] Yuanxi Guo,[1] and Rui Mao[1]

Abstract. The air pollution in Chinese Spring Festival (CSF) period over eastern China was investigated using the long-term observations from 2001–2012 over 323 stations. The dominant feature of the pollutants around the CSF holidays is the significant reduction of concentration. During ten-day period around the CSF (but excluding the Lunar New Year's Day, LNYD), PM_{10} experiences a reduction of −9.24%. In association with the aerosol reduction, temperature significantly drops over the eastern China. From the third day before the LNYD to the second day after, the daily mean temperature anomaly is −0.81°C and for no-rain days the anomaly is −0.85°C. The simultaneous anomalies of the daily maximum and minimum temperatures are −0.79°C and −0.82°C, respectively. From the third to seventh day after the LNYD, the significant negative temperature anomalies move out of China, extending to a broad area from South China Sea to the western North Pacific. Between the eighth and the twelfth day, the significant temperature anomalies can still be found over 140°E–160°E and 15°N–25°N. The reduced downward longwave flux might play an important role in holiday cooling. The possible atmospheric feedback is discernable. The thermal and circulation configure accompanying the cooling favors baroclinic interaction between upper and lower troposphere for the mid-latitude cyclone. The anomalous cyclone develops mature during the third to the seventh day after the LNYD, and disappears twelve days later. The anomalous northern winds in association with the cyclone decrease temperature and also help disperse the holiday aerosols over the eastern China.

1. Introduction

Eastern China is one of the most populated and rapidly developing regions in the world. The intense human activities led to substantial emission of aerosols and their precursors, making eastern China one of the heaviest sources of anthropogenic air pollutants since the early 1980s [*Qian et al.*, 2003, 2006; *Richter et al.*, 2005; *Chan and Yao*, 2008]. Previous literatures analyzed the long-term changes of the primary pollutants. *Lei et al.* [2011] estimated that from 1990 to 2005 the emission factors of $PM_{2.5}$ (aerosol particulate matters with a diameter $< 2.5\mu m$) and total suspended particulate from different industry sectors of China decreased by 7%-69% and 18%-80%, respectively. Similar decreasing in PM_{10} (particulate matters with a diameter $< 10\mu m$) was also reported [e.g., *Qu.*, 2010]. The increase of NO_2, SO_2, and primary carbonaceous aerosol are also reported based on different data sources [*Zhang et al.*, 2007; *Lu et al.*, 2010; 2011]. The trends might be complicated by the interaction of the emission, environmental factors such as monsoonal winds, and pollutant mass mode [*Zhu et al.*, 2012; *Wang et al.*, 2012a]. Even though, the short-term, anthropogenic high pollution episodes with serious environmental and healthy consequences are frequently observed. The short-term aerosol-meteorological interactions would help better understand the aerosol trends in China. One such phenomenon can be found in day-to-day co-variations of the daily air pollution and human activity. Regular human activities are tightly associated with the PM_{10} weekly cycles, yielding a PM_{10} peak in around Thursday [*Gong et al.*, 2006; 2007; *Choi et al.*, 2008; *Wang et al.*, 2012b]. This kind of 7-day variation is also reported in other regions in the world, though the mechanism is not well understood yet [*Sanchez-Lorenzo et al.*, 2012]. On the other hand, regular or occasional intense human activities involving the cultural events can also remarkably change the ambient air quality. For example, under condition of emission control management (including the reduction of factory emission and vehicle activity) during the 2008 Beijing Olympic Games, the background and urban site $PM_{2.5}$ concentration decreased by about 48%-56% over a large region around Beijing-Tianjing-Hebei urban agglomerations [*Xin et al.*, 2012]. In contrast, fireworks during cultural celebration and festivals cause air pollution and adverse health impacts as reported world-widely. For example, *Camilleria and Vella* [2010] observed that compared to the normal days the PM_{10} and metal concentrations were significantly higher involving the religious festival fireworks burning in Malta. Similarly, worse air quality caused by fireworks was observed in other European cities [e.g., *Harrad and Laurie*, 2005; *Drewnick et al.*, 2006; *Vecchi et al.*, 2008; *Moreno et al.*, 2010; *Crespo et al.*, 2012]. In North America during the 4th July holiday pollutants (magnesium, aluminum, lead, PM_{10}, etc) significantly increase [*Liu et al.*, 1997; *Carranza et al.*, 2001]. Case studies in India found that during Diwali festivals the effect of fireworks cause remarkably higher concentration of the air pollutants (SO_2, NO_2, $PM_{2.5}$, PM_{10}) in Indian cities such as Hisar, Lucknow, and Calcutta) [*Ravindra et al.*, 2003; *Barman et al.*, 2008, 2009; *Chatterjee et al.*, 2013].

[1]State Key Laboratory of Earth Surface Processes and Resource Ecology (ESPRE), Beijing Normal University, Beijing 100875, China (gdy@bnu.edu.cn)

[2]Department of Earth System Science, University of California, Irvine CA 92697 USA (wenshanw@uci.edu)

[3]Pacific Northwest National Laboratory, Richland, WA 99352, USA (yun.qian@pnnl.gov)

[4]Civil and Environmental Engineering, Carnegie Mellon University, Pittsburgh, PA 15213, USA (wenbing.cmu@gmail.com)

0148-0227/14/$9.00

Chinese Spring Festival (CSF, also known as the Chinese New Year or Lunar New Year) is the most important holiday for Chinese. Traditionally, holidays begin a couple of days before the Lunar New Year and end at the lantern day, lasting for about two weeks. The climax of the celebration is a display of fireworks and setting off firecrackers during the New Year's Eve. That causes severe ambient air pollution. For example, *Wang et al.* [2007] reported that there are higher levels of SO_2, NOx, $PM_{2.5}$ and PM_{10} in Beijing during fireworks of lantern day in 2006, and compared with normal days, the primary and secondary components of aerosols are five times higher. Based on 1994–2006 observations from thirteen monitoring sites around Taipei metropolitan area, *Tan et al.* [2009] found that the concentrations of NOx, CO, non-methane hydrocarbon, SO_2 and PM_{10} were lower in the new-year periods than in the non-new-year periods. *Zhang et al.* [2010] found that particle (diameter range of 10 nm to 10 mm) concentrations in Shanghai during the peak hour of firework celebrations in 2009 New Year were approximately 3 times higher than the day before. Recently, *Li et al.* [2013] reported that during the 2011 Chinese New Year, $PM_{2.5}$ is six times higher than that before and after the holiday over the Yellow River delta region. *Lin and McElory* [2011] analyzed the CSF events using NO_2 data and atmospheric chemical transport modeling and reported a reduction of the emission due to the slowdown of the holiday economy. Note that previous studies are based on single city or single event. Meanwhile the celebration of Spring Festivals involves urban and rural areas across the whole country.

It is unclear how the ambient air quality changes during the short-term Chinese Spring Festival periods over the country and whether the air temperature has detectable changes in association with the aerosol changes. The purpose of the present study is to investigate the short-term variations of PM_{10} pollution as well as the temperature co-changes during the holidays over the densely populated eastern China by employing air pollution observations from 323 pollution and 516 meteorological stations.

2. Data

The station dataset used in the present study consists of daily ambient air pollution index (API), daily SO_2 and NO_2 concentrations, and meteorological records. First, API data are obtained from the Ministry of Environmental Protection of the People's Republic of China and the Department of Environmental Protection for 14 provinces (Table 1). For a specific calendar day, the daily mean is the average from 12:00 Beijing local time of the previous day to 12:00 of the present day. Totally, there are 323 stations east of 100°E after excluding the duplicated sites, and their locations are plotted in Figure 1. The daily API is defined by two key parameters: the API type (which indicates the type of the leading pollutant SO_2, NO_2, or PM_{10}) and the non-dimensional index value (which is transformed from the pollutant concentrations). The maximum of API is set to 500. If the API is below 50, it is defined as a clean day and no pollutant type is set. According to the National Standard of the Ambient Air Quality in China, the concentration of the major pollutant can be derived from the API by using the formula: $C = C_L + (API\text{-}API_L)(C_U\text{-}C_L)/(API_U\text{-}API_L)$, where C is the concentration, API_U and API_L are the upper and lower standard API values, respectively corresponding to the upper and lower standard concentrations C_U and C_L in the same order (see also *Gong et al.* [2007] and *Qu et al.* [2010] for details). When deriving the concentration, the leading pollutant is set to PM_{10} for API$<$ 50 cases. Eighteen of the 24 stations in Sichuan Province, no pollutant type information are available. We simply set PM_{10} as the leading pollutant. Estimated from other 6 stations with full information in Sichuan Province, we found that the PM_{10} days accounts for about 72.5% of the total records in January-February. We also repeated our analysis excluding all stations of Sichuan Province and found a similar result. In addition, daily co-observations of the PM_{10}, SO_2, and NO_2 for 13 stations are also analyzed. These data are obtained from the municipal administration of environmental protection of 13 cities (Figure 1).

Daily meteorological observations are taken from China Meteorological Administration. Parameters used include the 2 meter dry-bulb temperature, precipitation, maximum temperature, and minimum temperature. We confined our analysis period to 2001–2012, same as for aerosol data. During this time period we selected 516 stations of which the data availability is above 95% during January and February (Figure 1), of which 129 stations are co-located with PM_{10}. The missing meteorological records are excluded from analysis.

The ERA-Interim reanalysis datasets from 2001–2012 are utilized, including the surface and pressure level parameters. The surface variables analyzed are 2 meter temperature and radiations. And the pressure level variables consist of temperature, geopotential heights, and horizontal winds. This dataset is of 1.5° spatial resolution and has 37 pressure levels in vertical direction [*Dee et al.*, 2011].

We employed the surface downward long-wave flux from the Modern-Era Retrospective analysis for Research and Applications (MERRA) from 2001–2012, which is a NASA reanalysis utilizing satellite observation derived from the Goddard Earth Observing System Atmospheric Data Assimilation System (GEOS-5). This hourly dataset is available with a resolution of 0.5° in latitude and 0.667° in longitude [*Rienecker et al.*, 2011].

3. Results

3.1. Background of climate and PM_{10} concentration

Prior to analyze the holiday variations in air pollution, we first examined the long-term mean background of ambient air pollution and climate. Given the fact that the calendar days of the Chinese New Year all occur within January and February (Table 2), we computed the long-term background for January-February from 2001 to 2012. Because the eastern China covers a quite large area with different climate background from north to the south, we separately examined the sub-regional climates and PM10 concentration (similar to *Qu et al.* [2010]). The mean January-February temperature for the stations north of 35°N is −8.7°C. For stations south of 28°N is 11.7°C. And the mean temperature in the central China is 3.1°C. Meanwhile, the regional mean precipitation amount increases from 9.8mm in the northern China to 70.2mm in the central China, and to 82.3mm in the southern China. The corresponding rainy days are 7.2, 16.3, and 17.7 days respectively. The mean surface wind speeds for three sub-regions are similar, varying between 2.0–2.4ms^{-1}. It is different from spring when frequent windy days occur in north. Thus, the northern China is a region with cold and dry climate, while the central and southern China are relatively warmer and wetter. This is an important factor relating to the background concentration of the ambient atmosphere PM_{10} as shown below.

Figure 1b displays the spatial distribution of the long-term means of the January-February PM_{10} concentration for 323 stations. The regional feature among sites is somewhat complex, depending on the geographical, social and economical conditions. For example, there are some sites of 40–60μgm^{-3} north of 40°N, which are located in the pastoral zone in Inner Mongolia. The outstanding minimum site ($<$ 40μgm^{-3}) in north China is Wutai mountain station (39.0°N, 113.6°E, 1700m above sea level). Generally,

PM_{10} decreases from a higher concentration in the north to a lower concentration in the south. Mean and standard deviation of PM_{10} for northern, central, and southern China are $120.1 \pm 81.2\mu gm^{-3}$, $102.4 \pm 57.2\mu gm^{-3}$, and $69.3 \pm 38.2\mu gm^{-3}$, respectively. Seasonal cycle of the PM_{10} concentration is also plotted in Figure 1c. Boreal winter (December-January) has the maximum of $110.0\mu gm^{-3}$, while the boreal summer (July-August) has the minimum of $65.1\mu gm^{-3}$. Based on less surface station records, previous studies also reported that high PM_{10} concentration appears in boreal winter and spring, and the lowest concentration appears in summer [e.g., *Song et al.*, 2009; *Qu et al.*, 2010]. Thus, the long-term means derived for 323 stations indicate a high PM_{10} background in boreal winter, which is featured by a dirtier-north-cleaner-south distribution. And the CSF periods occur in a season of high concentration background.

3.2. Lower PM_{10} concentration in holiday periods

In order to examine the PM_{10} variations around the CSF period, here we utilized the composite analysis. Because the New Year day is determined according to the traditional lunar calendar, the date changes from year to year. During the analysis period 2001–2012 the LNYD varies between 22 January and 18 February (Table 2). The LNYD is denoted as day 0, the day before and after the LNYD is denoted as day −1 and day +1, respectively. Two days before and after are as day −2 and +2, and so on. We tried to use a longer time lag and found that the significant changes just occur in a couple of days around the LNYD. Furthermore, as be indicated in next sections the meteorological anomalies beyond 12 days are not discernable. For simplicity here we analyze the period from day −12 to day +12. For a given day (e.g. day −1) in a specific year (e.g., 2001), the PM_{10} concentration is the average of all the available stations. For the analysis period 2001–2012, there are 12 regional means, and are averaged to obtain the long-term daily mean. The uncertainty of the means is estimated using standard error (SE), smaller SE suggesting less sampling mean error. Composite of other parameters is dealt with in the same way. Note that even the dust aerosols in East Asia may be transported by westerly from upstream direction [e.g., *Huang et al.*, 2008], its influence on the results could be negligible because our composite focusing on the daily variations around the LNYD.

The climate background differs from north to the south, which may influence the aerosol scavenging. We examined the PM_{10} variations for three sub-regions from southern China to the northern [e.g., *Qu et al.* 2010]. Computed from 60 stations south of 28°N, the mean PM_{10} concentration in days −10 to −5 is as high as $66.93\mu gm^{-3}$, while the value in day +2 is only $47.3\mu gm^{-3}$, being decreased by $19.2\mu gm^{-3}$. For the 157 stations north of 35°N, the PM_{10} changes from $141.1\mu gm^{-3}$ to $117.1\mu gm^{-3}$, decreases by $24.1\mu gm^{-3}$. Between them, the mean PM_{10} concentration of 106 stations changes from $112.8\mu gm^{-3}$ to $88.44\mu gm^{-3}$, being a reduction of $24.4\mu gm^{-3}$. For all three sub-regions the abrupt rises of PM_{10} concentration occur in day 0, accompanying the intense usage of firework. The PM_{10} variations for three sub-regions are generally similar, suggesting a national-wide holiday phenomenon. The similarity of regional PM_{10} variations during the holiday period encourages us to carry out a composite for all 323 stations (Figure 2a). Given the regional similarity, here we did not consider the area weight when making the regional means even there are denser stations in northern China. Generally, the PM_{10} concentration before the LNYD is relatively high. The mean value for day −10 to day −5 is $107.6\mu gm^{-3}$, but the concentration for day +5 to day +10 is $92.5\mu gm^{-3}$. This declining trend may partly be due to the seasonal change from January to February (see Figure 1c). However, an interesting feature revealed by the composite is the dramatic drop from $104.5\mu gm^{-3}$ in day −5 to $91.5\mu gm^{-3}$ in day −1, which is followed by an abrupt jump to $123.8\mu gm^{-3}$ in day 0, and then a gradually increasing from the minimum of $83.1\mu gm^{-3}$ in day +2 to a higher $97.9\mu gm^{-3}$ within a week.

Note that there is evident seasonal tendency, which may bring unexpected variations when different calendar days are used to make composite. For clarification, here we repeated the composites but based on the daily PM_{10} anomalies. We first removed the seasonal cycle by subtracting the long-term average from the daily concentration to yield the daily PM_{10} anomalies (ΔPM_{10}). Then the means of the anomalies are computed from day −12 to day +12 and shown in Figure 2b. Note that the New Year day peak can result in notable bias for the estimation of seasonal cycle and the corresponding anomalies, thus we excluded all Lunar New Year Days when estimating the climatological mean concentration. The anomaly composites reveal that the LNYD peak is still the most outstanding departure, meanwhile the anomalies in four days before the LNYD are evidently below the normal. The negative anomalies in day −4 to day −1 are impressing with a mean anomaly of $-9.71\mu gm^{-3}$. As the climate mean concentrations for the period varies from $101.21\mu gm^{-3}$ in day −4 to $97.21\mu gm^{-3}$ in day −1, the corresponding percentage reduction of PM_{10} in these four days is from −8.54% to −14.40%. The minimum anomaly of $14.86\mu gm^{-3}$ in day −2 is about 15.1% lower than the normal. On average PM_{10} for these four days is 12.40% lower than the background. The statistical significance of anomalies in day −4 to day −1 was also estimated using a left-tail t-test. The null hypothesis that the anomalies during these days are similar to the normal is rejected at the 0.01 level. The negative anomalies are interrupted by the anomalous ΔPM_{10} peak of $26.75\mu gm^{-3}$ in the LNYD, which is an increment of 27.87% above the normal. The negative departures after the LNYD are smaller than the days before. The ΔPM_{10} of $10.6\mu gm^{-3}$ in day +2 is evidently low (−11.21%), but not the lowest, which is followed by the gradual increasing to normal. These consecutive anomalies from day +2 to day +5 seem to be indicative of robust and stable signal. We took all samples from day +2 to day +5 during the analysis period, and estimated their significance under the null hypothesis that they do not statistically differ from zero. We employed a left-tail t-test, and found that the null hypothesis is rejected at the 0.05 level. On average, the PM_{10} reduction during day +2 to day +5 is −7.17%. During a 10-day period around the CSF period (from day −4 to day +5 but excluding day 0), the ΔPM_{10} experiences a reduction of −9.24%.

3.3. Variations of SO_2 and NO_2 concentration

The SO_2 and NO_2 are important air pollutants and precursors of aerosols in China. Here we collected daily SO_2 and NO_2 data for 13 stations, including Huaihua (27.7°, 110.0°E), Guangzhou (23.2°N, 113.3°E), Yinchuan (38.5°N, 106.2°E), Xi'an (34.3°N, 108.9°E), Wuhan (30.6°N, 114.1°E), Tianjin (39.1°N, 117.1°E), Shaoxing (30.0°N, 120.3°E), Shanghai (31.2°N, 121.4°E), Nanning (22.8°N, 108.4°E), Guiyang (26.6°N, 106.7°E), Harbin (45.8°N, 126.8°E), Ningbo (29.9°N, 121.6°E), and Weinan (34.3°N, 109.3°E). Simultaneous records of PM_{10}, SO_2 and NO_2 are available, except for Harbin of which NO_2 data are not provided. The daily PM_{10} concentration is found to vary with SO_2 and NO_2 tightly. For example, *Wang et al.* [2012b] analyzed the day-to-day variations in PM_{10}, SO_2 and NO_2 in the southern China during September-November, and found all have obvious peaks on around Thursday and minima in weekends. We computed the Pearson correlations of PM_{10} with SO_2 and NO_2 using daily observation for 13 stations. During non-holidays

(day −10 to day −5) the correlation between PM_{10} and SO_2 is +0.61. And the correlation with NO_2 is +0.45, both significant at the 0.01 level. This consistently indicates that the daily variations of PM_{10}, SO_2 and NO_2 in non-holidays are highly positively correlated. How about the situation around the CSF periods? We performed the composite analysis for SO_2 and NO_2 (Figure 3). Generally, the SO_2 and NO_2 decrease from higher value in days −10 to −5 to a minimum in day +2. The SO_2 decreases from 63.0μgm^{-3} to 48.3μgm^{-3}. And the NO_2 changes from 57.0μgm^{-3} to 39.5μgm^{-3}. Although the urban population and geographical locations differs much, the temporal features of the three major pollutants in the CSF periods are similar among cities. These features are also similar to *Tan et al.* [2009]'s finding that a general reduction of PM_{10}, SO_2 and NOx in the CSF periods around the urban area of Taipei during 1994–2006. The abruptly soaring concentrations of PM_{10} and SO_2 in day 0, however, notably differ from NO_2. A relatively high NO_2 (57.3μgm^{-3}) appears in day −2, but there is no peak in the LNYD. The NO_2 in day 0 is 44.1μgm^{-3} and close to the concentration of 45.3μgm^{-3} in day −1 and 44.7μgm^{-3} in day +1. Based on above observation analysis we may conclude that the aerosol concentration (PM_{10}, SO_2 and NO_2) over the whole eastern China is featured by a notable reduction during the CSF holiday period with unusually high NO_2 peak two days before the LNYD and outstanding PM_{10} and SO_2 maxima in the LNYD.

The different temporal features of NO_2, PM_{10} and SO_2 around the CSF (particularly their peaks) are likely related to the different holiday emission sources. Since the major source of NO_2 in China is motor vehicles [e.g., *Saikawa et al.*, 2011] and main anthropogenic NOx source in China is power plant [*Zhang et al.*, 2009; *Wang et al.*, 2010], a reduction of urban vehicle activity and power production might help reduce NO_2 concentration. The relative higher NO_2 value in day -2 seems be related to the enhanced vehicle activity for urban shopping and road transportation preparing for the CSF. Also we would like to point out that the NO_2 composites contain relatively large noise due to limited data samples. On the other hand, in the New Year Eve the intense burning of fireworks across the country causes simultaneous air pollution, yielding LNYD PM_{10} and SO_2 peaks. The increased demand for heating may also enhance the SO_2 emission. It is interesting to note that the air pollution feature in the CSF period differs from holiday pollution in neighbor countries. For example, the in-phase variations for SO_2, NO_2 and PM_{10} are observed in Indian Diwali festivals in Hisar city in November 1999 [*Ravindra et al.*, 2003], where the maximum NO_2 concentration appears one day after the festival. *Barman et al.* [2008] also reported simultaneous increases of PM_{10}, SO_2 and NO_2 in Diwali day in Lucknow City. Additionally, the involved species transformation would make thing complex. For example, *Nishanth et al.* [2012] found that the NO_2 increase in Kerala during Vishu festivals on April 14th and 15th in 2010 and 2011 corresponds well to the production of O_3 during the firework display. While *Li et al.* [2013] indicated that the fireworks emissions during the CSF period may significantly change the atmospheric transformation pathway of SO_2 to sulfate. Looking into differences between daytime and nighttime variations in PM_{10}, SO_2, and NO_2 may be helpful for identifying the sources of these pollutants (e.g., fireworks at night, vehicle emissions during the day) and their possible meteorological influence.

Although the firework display is responsible for the PM_{10} and SO_2 sharp peaks in day 0, we argue that the holiday firework emissions during the whole holidays may not be so important because the firework released pollutants are of short-time impact, after the maximal firework displaying in night the airborne particles dissipate quickly [e.g., *Wang et al.*, 2007; *Vecchi et al.*, 2008] so that the outstanding PM_{10} peak in day 0 turns negative anomaly in day +1 (Figure 2b). More importantly, the economic slow-down during the holidays reduces emissions. Using three different approaches considering the thermal power generation, satellite retrieval products, statistical and modeling attributing, *Lin and McElroy* [2011] estimated that the economic downturn during the celebrating CSF was responsible for a notable reduction in anthropogenic emission. According to their estimations for 2005, 2007, 2008 and 2010, the CSF contributes a NOx emission reduction of 12%. And the 2009 CSF contributes a reduction of 10%. Interestingly, we note that their estimations are comparable with our estimation of the PM_{10} reduction derived from 323 station measurements (−9.24% for days −4 to +5 excluding day 0). It is acknowledged that day-to-day variations of PM_{10} and major pollutants are significantly correlated [e.g., *Wang et al.*, 2012b], and our analysis also confirms the tight in-phase variations among PM_{10}, SO_2 and NO_2. Thus the holiday economic and industrial slowdown may also contribute much of the observed CSF PM_{10} reduction.

3.4. Observed station temperature cooling

Above analysis display distinguished holiday variations of air pollution during the CSF periods, a new question is how the air temperature changes with holiday aerosols. Here we examined the variations of the surface air temperature by making composites, similar to the analysis of ΔPM_{10}. Here all composites for meteorological parameters are based on anomalies. For example, the 2001–2012 long-term mean is subtracted from the daily temperatures to obtain the temperature anomalies (ΔT). Then the anomalies are employed in the temperature composite analysis, including daily mean temperature (ΔTavg), maximum temperature (ΔTmax), and minimum temperature (ΔTmin).

We investigated the temperature anomalies for 516 stations with all observation days utilized. There are similar temporal features among ΔTavg, ΔTmax and ΔTmin with evident cooling observed in around the CSF. The largest negative anomalies tend to occur in the period from about day −3 to day +2. The ΔTavg minimum of −1.09°C, the ΔTmax minimum of −1.17°C and the ΔTmin minimum of −1.03°C appear in day −2, day −3 and day −1, respectively. The daily mean temperature during days −3 to +2 is 0.81°C lower than normal, significant at the 0.01 level as estimated from a left-tail *t*-test. At the same time, the maximum and minimum temperatures are 0.79°C and 0.82°C cooler, statistically significant too. These lower-than-normal temperatures apparently appear concurrently with lower PM_{10} concentration anomalies. Their co-variations suggest an in-phase relationship. By comparing Figure 2b and Figure 4a, we could find that both variables decrease from a relatively high values in day −6 to a minimum in day −2, then together increase to a high value in day 0, and then lower values appear in days +1 and +2, which followed by gradual increase within the next 5–6 days. We analyzed the composites using the 129 PM_{10} collocate stations, and found similar features (Figure 4 and Table 3). The negative ΔTavg averaged from 129 stations is −0.85° C. Precipitation can efficiently remove the airborne pollutants, thus reduce the aerosol concentration. On the other hand the precipitation-related synoptic system tend to bring temperature down. Therefore, precipitation impacts the temperature-PM_{10} relationship, even though the precipitation occurs infrequently in winter. For clarification we repeated the composites for 516 stations as well as for 129 collocate stations but excluded all precipitation days. We found that the temporal features are almost the same and during days −3 to +2 there are slightly cooler temperature anomalies. The significant (at the 0.01 level) anomaly means for 516 stations and for 129 stations are −0.85°C and −0.89°C, respectively (Figure 5, and Table 3).

As demonstrated in the previous section, the holiday reduction of PM_{10} concentration is observed in the densely populated eastern China. If the temperature cooling is physically aerosol-related, we would expect consistent negative anomalies from northern China to the southern. We computed the means of ΔTavg from day -3 to day $+2$ and estimated their statistical significance level using a left-tail t-test station by station. Results are shown in Figure 6. The majority of the temperature anomalies are of negative sign. Among 516 stations, there are 30 stations with positive signs but none of them are significant at the 0.1 level. Of the 486 stations with cooling temperature anomalies, 390 stations are significant at the 0.1 level, and 331 significant the 0.05 level. The cooling centers are located in two regions, one in the central China in about 25°N–35°N east of 110°E, and another center appears in northeastern China (about 40°N–45°N east of 120°E). The results derived from no-rain days are similar (Figure 6b). There are 344 stations with cooling temperature anomalies significant at the 0.1 level, and 276 stations significant at the 0.05 level.

3.5. ERA-Interim surface temperature anomalies

Does the observed holiday cooling occur only in eastern China or is a phenomenon simultaneously appearing in other countries? And such cooling can be reproduced in reanalysis data? Firstly, we assessed the robustness of the holiday cooling by comparing ERA-Interim reanalysis 2m temperature over East Asia. Since the reanalysis grid points are not exactly collocated with the urban area, this helps remove the local factors' influence such as the urban-heat-island effect. We computed the mean daily ΔTavg by averaging all 218 grids located within China east of 100°E, and found a variation feature similar to station observation with a minimum of -1.2°C in days -3 and -2. The mean anomaly from day -3 to $+2$ is -0.81°C, same as station observation and significant at the 0.01 level. The significant negative temperatures for daytime (mean of 00:00UTC and 06:00UTC) and nighttime (mean of 12:00UTC and 18:00UTC) are -0.82°C and -0.80°C, respectively. Secondly, we investigated the spatial distribution of the ΔTavg for each grid over East Asia. Figure 7 displays the results for nighttime and daytime. In both cases the majority of the significantly negative temperature anomalies are located in the dense populated eastern China, almost identical to the station observations. Interestingly, the significant grids disappear out of China's border to the east and the north sides. The two cooling centers in the central and northeastern China are similar to the station data, too. In the downstream direct, there are significant anomalies appearing in the Sea of Japan/East Sea, and Yellow Sea. These maritime cooling might be due to the propagation from the neighboring northern and northeastern China. The similarity between reanalysis and station temperature is indicative of the nation-wide holiday cooling appearing in both urban and non-urban areas.

As shown in Figure 8, the significant negative surface temperature anomalies in eastern China approach to the normal after day $+3$ but the significant cooling signals can be tracked over the oceans. Along with the prevailing atmospheric circulation the temperature anomalies move southeastward. In days $+3$ to $+7$, the significant cooling grids are located over a broad area extending from South China Sea to the western North Pacific south of Japan. The anomaly center is between 130°E–150°E and 25°N–35°N where the negative temperature departures are of -0.4°C to -0.8°C. Even 8–12 days later, the significant cooling can still be found over 140°E–160°E and 15°N–25°N though the anomalies are evidently smaller (Figure 8).

3.6. Vertical profile of the lower troposphere cooling

We note that during the CSF period the daily temperature and PM_{10} experience an evident in-phase variation. We speculate that holiday variations of aerosols may impact temperature through modulating radiation by direct or/and indirect effects. The reduction of aerosols (in particular the absorbing aerosols) in the holidays should cool the nighttime lower troposphere and the surface, as well as the daytime boundary layers. Meanwhile the corresponding daytime surface temperature depends on the net budget of the short- and long-wave fluxes. The loss of downward longwave radiation, if cannot be compensated by the shortwave radiation, would result in a cooler surface. The temperature vertical profiles could provide useful information for better understanding of the radiation changes. Here we examined the vertical profiles of the temperature anomalies in both daytime and nighttime during days -3 to $+2$. Averaged over 218 grids in eastern China, we plotted the temperature anomalies below 500hPa level (Figure 7e and f). In nighttime the significant negative temperature anomalies appear below 850hPa. The negative anomaly at 875hPa is -0.68°C, for lower levels are -0.72°C. The mean for these layers is -0.72°C. In daytime, significant cooling in 850hPa is -0.73°C, and at 1000hPa is -0.84°C. Averaging from all layers between 850hPa and 1000hPa yields a value of -0.82°C. We note that the boundary layer and neighboring free atmosphere in daytime show larger cooling than at night (0.1°C cooler). And the daytime cooling spreads to higher altitude than at night. The aerosols released by fireworks at night are likely to contribute to this cooling phenomenon. We examined the temperature anomalies in the New Year's Eve. As shown in Figure 7, comparing to the mean temperatures for days -3 to $+2$ the temperature cooling in New Year's Eve is obviously smaller, implying an additional warming. The evident warming (> 0.2°C) appears between 850hPa and 600hPa with the maxima of 0.3°C from 775hPa to 650hPa. The profile becomes somewhat vertically uniform in the following daytime, probably due to the stronger vertical mixing. Generally speaking, the lower troposphere and surface cooling is consistent with the simultaneous reduction of aerosol concentration in the holidays.

In concern of the aerosol direct and indirect effects the downward longwave are essential for surface temperatures [e.g., *Huang et al.*, 2006a]. The direct effect of aerosols in winter would play a more important role in influencing daily temperature [*Gong et al.*, 2006]. Recent observation shows that longwave radiative effect of large size dust particles in dry northwest China ranges from 2–20 Wm^{-2} [*Hansell et al.*, 2012]. And the aerosol backscattering of the long-wave flux can be a few watts [*Dufresne et al.*, 2002]. Through altering the liquid cloud properties via the first indirect effect, the aerosol can also produce long-wave warming of the surface [e.g., *Dan and Vogelmann*, 2006]. In northwestern China about one third of the dust aerosol radiative cooling effect is compensated by its longwave warming effect [*Huang et al.*, 2009]. Due to the lack of dense and high-resolution station radiation data, we cannot make estimation to what extent the holiday aerosols alter the radiation budget over China. Alternatively, here we investigated the ERA-Interim reanalysis longwave fluxes. According to the station temperature and ERA-Interim 2m temperature distribution, we selected grids east of 100°E located within China. Interestingly, we found that the downward longwave radiations in daytime and nighttime are evidently lower than the normal in days -4 to $+4$ (Figure 7). On average the anomaly for daytime and nighttime is $-4.1Wm^{-2}$ and $-4.0Wm^{-2}$, respectively. Both are significant at the 0.01 level by a left-tail t-test. The maximum drops of $-6.7Wm^{-2}$ for daytime and $-8.4Wm^{-2}$ for nighttime both occur in day -2, being coincident with the observed surface PM_{10} and temperature minima. In addition, the daytime surface net radiations (the net shortwave

plus the net longwave) are of evident negative anomalies in days −3 to −1, with an average of $-4.34\mathrm{Wm}^{-2}$ but not statistically significant (figure not shown). These are physically consistent with the observed holiday aerosol reduction and the simultaneous temperature cooling in the boundary layer and surface. It should be pointed out that here we used ERA-Interim 2m temperatures at step 0 for 00:00UTC, 06:00UTC, 12:00UTC and 18:00UTC. These step 0 outputs are analyzed parameters, while the radiations of 00:00UTC at steps 3–9 used for daytime and 12:00UTC at steps 3–9 used for nighttime are forecast. Anomalies of radiations in Figure 7 are not real observations. We additionally analyzed the MERRA surface downward long-wave flux from 2001–2012. Here we selected 1456 grids within eastern China (east of 100°E). The daily anomalies are averaged and plotted together with the ERA-Interim radiation in Figure 7. Daytime value is the average from 00:00 UTC to 10:00UTC, and the nighttime value is the average from 11:00UTC to 23:00UTC. The temporal variations of MERRA resemble those of ERA-Interim quite closely. Relatively low values also appear in days −4 to +4. But the holiday anomalies in MERRA are not statistically significant. Anyway, station radiation observations are in need to verify the holiday radiation budget and its roles involving in the surface and boundary layer cooling.

3.7. A possible atmospheric feedback

We note that coincident with the boundary layer and surface cooling, there are significant negative temperature anomalies in middle troposphere in days −3 to +2 (Figure 9). The upper level atmospheric anomalies follow the surface cooling and moves to 130°–150°E with maxima between 700hPa and 850hPa in days +3 to +7, and extend to east of 160°E in days +8 to +12. At the same time the cooling centers are accompanied by collocate negative geopotential heights, implying an anomalous synoptic cool-core low pressure develops in the East Asia during the holiday periods. Here we suppose that there is atmospheric response to the holiday cooling and the atmospheric circulation further alter the surface temperature.

Because the maximum boundary layer and surface cooling appear in days −3 to −1, we first investigated the simultaneous geopotential height anomalies. As shown in Figure 9d, the anomalies are of −1.2°C to −1.6°C below 850hPa between 110°E–120°E, and of −0.8°C to −1.2°C between 120°E–135°E. Geopotential heights aloft the cooling center are negative, implying lower pressure in the troposphere with the center in about 250hPa. Interestingly, the axis of the anomalous pressure is not perpendicular. It tilts from about 140°E at 700hPa to 110°E at 250hPa. This means in lower troposphere there is enhanced cool thermal advection behind the axis of the low pressure. At the same time, because the upper troposphere lower pressure center is located to the west of the surface cooling center, there is northeastward airflow ahead of trough in the mid-upper troposphere between 120°E and 140°E. This kind of circulation and thermal settings implies constructive baroclinic interaction between upper and lower troposphere, tends to enhance the development of mid-latitude cyclone system [*Hakim et al.*, 2003]. The anomalous cyclone develops mature in days +3 to +7 with the center being located between 140°E and 150°E along 30°N. In days +8 to +12 the center of the cyclone moves to around 25°N and 150°E and its intensity weakens. As the anomalous cyclone moves eastwards, the cool temperature carried by the northern winds behind the cyclone moves together and gradually spreads from the middle troposphere to the 850hPa (Figures 9 and 10). Note that the East Asia is located to the western flank of the cyclone, thus there are anomalous northern winds from day −3 to day +12. This helps decrease the temperature as well as disperse the holiday aerosols. During days +13 to +17, the cyclone disappears, and the southward airflow anomalies over East Asia is replaced by northward wind anomalies (figure not shown), and there is no significant geopotential height anomaly over the western North Pacific.

3.8. Discussion

Regarding the observed holiday aerosol reduction and temperature cooling, there are some issues should be discussed.

The weather activity plays dominant role in daily temperature fluctuation. Our analysis may be biased by weather extremes. In practice there are two ways often used to suppress/exclude the weather disturbances. (i) To enhance the signal-to-noise ratio by using more samples to smooth out the random synoptic noise. We examined the temperature variations for a long-term period from 1979–2012 for both station observation and ERA-Interim reanalysis and found the significant holiday cooling is more evident than the results estimated from a short period data from 2001–2012 (Figure 11). The cooling appears in a longer period, spanning from day −4 to day +4 with a small increase in days 0. Mean daily temperature anomalies from days −4 to +4 is −0.97°C, when all rainy days are excluded ΔTavg is −0.99°C. And (ii) to exclude weather events. The abrupt large temperature drops caused by cold surges are frequently observed in winter. We tried to exclude these weather disturbances, particularly the cold surges. Here we identify a weather disturbance according to the temperature difference in two consecutive days ($|\mathrm{Tavg}_i - \mathrm{Tavg}_{i+1}|$, i is a calendar day) and the temperature anomaly ($|\Delta\mathrm{Tavg}|$)[c.f., *Wang and Ding* 2006; *Park et al.*, 2011; *Ding* 2013]. A disturbance is defined as $|\Delta\mathrm{Tavg}| > 5$°C or $|\mathrm{Tavg}_i - \mathrm{Tavg}_{i+1}| > \mathrm{T_o}$, where $\mathrm{T_o}$ is a threshold (for example, 6°C). For a specific station and a specific new year, if there is a weather disturbance in period from days −4 to +4, then the data for this year are excluded. We tried different $\mathrm{T_o}$ varying from 6°C to 3°C. As a lower threshold (such as 3°C) employed, in which moderate and weaker disturbances might have been identified and excluded, the cooling signals around the CSF actually become more stable and the corresponding statistical significance is also improved (Figure 12). Similar features remain when 34-year of data is utilized. These analysis support the robustness of the holiday cooling.

In our analysis we proposed a hypothesis that the holiday cooling may impact the regional circulation (i.e., an anomalous cyclone). However, it is possible that the observed aerosol reduction and temperature cooling are both caused by the passage of the cyclone/front. For clarification, we performed additional analysis based on (i) long-term data and (ii) time-lag composites. Using data from 1979–2012, we found the anomalous cyclone around the CSF are quite similar to that derived for 2001–2012. More importantly, we note that during days -4 to 0 there is no anomalous cyclone over East Asia (Figure 13), meanwhile the surface temperature significantly lower than normal. In days 0 to +4, a large anomalous cyclone appears over 110°E–160°E and 15°N–40°N, and this cyclone moves eastward to 120°E–170°E in days +4 to +8. These features are also outstanding in the data period of 2001–2012. As shown in Figure 13, during days −4 to 0, there are significant negative anomalies of 500hPa heights but no cyclone. Anomalous western winds appear in south of the height anomalies, at the same time anomalous eastern winds appear in the northern side. In contrast, in days 0 to +4 a strong cyclonic circulation dominates the East Asia and northwestern Pacific. This is convincing evidence that the cooling in days −4 to 0 would not be caused by the passage of cyclones. Instead, the obvious delaying appearance of the cyclone in days 0 to +4 is likely indicative of the atmospheric response

to the cooling. We note that there are a few works addressing the synoptic scale circulation anomalies caused by aerosol radiative effects. For example, *Jones et al.* [2004] reported that the dust aerosols in northern Africa significantly change the amplitudes of the downstream easterly waves in a couple of days where the dust heating plays essential role, while in our cases the cooling plays role. Based on the observational data *Ding et al.*[2013] reported that the pollution caused by agricultural burning and fossil fuel combustion in some provinces over East China results in significant modification of regional daily temperature and precipitation through pollution-boundary layer dynamics and aerosol-radiation-cloud feedbacks. In addition to the direct- and semi-direct radiation impacts on meteorology, numerical experiments with cloud microphysical processes show that the Asian pollution invigorates weather activities along the North Pacific storm tracks [*Zhang et al.*, 2007; *Wang et al.*, 2014]. Anyway, the holiday cooling-meteorology interaction is a challenge topic, and the responsible mechanisms require more detailed analysis and numerical modeling.

The aerosol-radiation interaction and aerosol-cloud/ precipitation interaction are complicated, causing complex aerosol-temperature relationship [*Boucher et al.*, 2013]. It seems no sole effect can explain daytime cooling. Aerosols can cool surface by direct effects. However, when more factors considered the situation gets complex. The direct radiative forcing is not necessary an indicator of surface temperature cooling response [e.g., *Hansen et al.*, 1997]. For the large particles the longwave radiation may be nonnegligible. For example, in northwestern China the dust aerosol radiative cooling effect is notably compensated by its longwave warming effect [*Huang et al.*, 2009]. Meanwhile the semi-direct effect can significantly change the low cloud and the albedo but not largely change the outgoing longwave radiation, resulting in a warming effect. The semi-effect in dry climate background (such as northern China) may play significantly roles in radiation budget [*Huang et al.*, 2006b]. Thus the ERA-Interim net radiation of $-4.34\mathrm{Wm}^{-2}$ in days -3 to -1 which is consistent with the daytime surface temperature cooling, would be a result of different effects. Although the decreases in the aerosol can result in either an increase or a decrease in aerosol-cloud related forcing, depending on the particular environmental conditions [*Boucher et al.*, 2013], we guess the aerosol's cloud life-time effect plays a role in the holiday nighttime cooling. The relative humidity between 600-850hPa is obviously less than normal, being an indicator for less mid- to low cloud. Less cloud surly results in cooling at night, but not sure during daytime. Note there are large uncertainties in aerosol-radiation interaction and aerosol-cloud interaction. Based on the station observation data and statistical analysis, we cannot prove the aerosol's impacts, nor can separate the possible meteorological feedback. How anthropogenic holiday aerosol impacts meteorology and how atmosphere feeds back remains a challenge needs both specific observation and numerical modeling.

In addition, anthropogenic heat is an important forcing of meteorology, especially in the urban and city-cluster and downwind regions [*Flanner*, 2009]. Recent studies [e.g. *Yang et al.*, 2014] also showed very high anthropogenic heat was released from the eastern China that can significantly modify the surface temperature [*Feng et al.*, 2012; 2014]. The anthropogenic heat should be significantly reduced during the CSF periods, which could be one important factor to influence the large scale air temperature. Its contribution to the observed holiday cooling needs further study.

4. Conclusion

Based on longer than decade observations of the station air pollutants over the eastern China, we found that the concentration of major air pollutants have significantly decreased around the CSF holidays. During day -4 to day -1, PM_{10} is 12.40% lower than normal. The negative anomalies are interrupted by rapid increment of 27.87% in the Lunar New Year Day. PM_{10} experiences continuous negative anomalies from day $+2$ to day $+5$ with a mean reduction of -7.17%. During the 10-day period from day -4 to day $+5$ (excluding day 0), the PM_{10} anomalies show an evident reduction of -9.24%. Similarly, the SO_2 and NO_2 decrease from high values in normal days to a holiday minimum. This amount of aerosol reduction is similar to the emission reduction due to the economic slowdown during the holidays [*Lin and McElroy*, 2011]. Meanwhile the intense usage of firework and active transport seems responsible for the different short-term peaks of PM_{10}, SO_2 and NO_2.

In association with the aerosol reduction, temperature significantly cools over the eastern China during days -3 to $+2$. The mean Tavg, Tmax and Tmin anomalies for 516 meteorological stations are -0.81°C, -0.79°C, and -0.82°C respectively. When rainy days excluded, the corresponding anomalies are -0.85°C, -0.93°C, and -0.78°C. The majority of the significant cooling is located within the densely populated eastern China. The spatial patterns are quite similar between station observation and ERA-Interim reanalysis dataset, implying the temperature anomalies are nation-wide phenomenon appearing in both urban and non-urban areas. The surface and boundary layer cooling are observed in both daytime and nighttime. The reduced downward longwave flux might play an important role in temperature cooling. During day $+3$ to day $+7$, the negative temperature anomalies move out of China, appearing over a broad area extending from South China Sea to the western North Pacific with a cooling center of -0.4°C to -0.8°C between 130°E–150°E and 25°N–35°N. The significant cooling can still be found over 140°E–160°E and 15°N–25°N during day $+8$ to day $+12$.

The simultaneous atmospheric circulation anomalies are analyzed, and found there are discernable atmospheric anomalies. Accompanying the lowest PM_{10} anomalies in day -3 to day -1, there are strongest simultaneous cooling in surface and boundary layer. At the same time in the mid-high troposphere there are negative geopotential height anomalies which are located slightly to the west of the lower troposphere cooling center. The thermal and circulation configure favors typical baroclinic interaction between upper and lower troposphere for the mid-latitude cyclone. The anomalous cyclone develops mature in day $+3$ to day $+7$ with a center between 140°E and 150°E along 30°N. In day $+8$ to day $+12$, the cyclone weakens and moves to around 25°N and 150°E. In association with the cyclone development the cool temperature anomalies propagate gradually from mid-troposphere to the lower levels. The cool thermal advection behind of the cyclone, in turn, helps maintain the troposphere cooling and disperse the holiday aerosols.

Acknowledgments. This research was supported by projects NSFC-41321001 and NSFC-40975043. Gong DY was supported by 2012CB955302. The contribution of Yun Qian in this study is supported by the U.S. Department of Energys Office of Science as part of the Regional and Global Climate Modeling Program. The Pacific Northwest National Laboratory is operated for DOE by Battelle Memorial Institute under contract DE-AC05-76RL01830. ERA-Interim reanalysis data used in this study were obtained from ECMWF at http://www.ecmwf.int/.

References

Barman, S. C., R. Singh, M. P. S. Negi, and S. K. Bhargava (2009), Fine particles (PM2.5) in ambient air of Lucknow City due to fireworks on Diwali Festival, *Journal of Environmental Biology*, **30**, 625-632.

Barman, S.C., R. Singh, M. P. S. Negi, and S. K. Bhargava (2008), Ambient air quality of Lucknow City (India) during use of fireworks on Diwali Festival, *Environmental Monitoring and Assessment*, **137**, 495-504.

Boucher, O., D. Randall, P. Artaxo, C. Bretherton, G. Feingold, P. Forster, V.-M. Kerminen, Y. Kondo, H. Liao, U. Lohmann, P. Rasch, S.K. Satheesh, S. Sherwood, B. Stevens, and X.Y. Zhang (2013), Clouds and Aerosols. In: *Climate Change 2013: The Physical Science Basis*. Stocker, T.F., D. Qin, G.-K. Plattner, M. Tignor, S.K. Allen, J. Boschung, A. Nauels, Y. Xia, V. Bex, and P.M. Midgley (eds.). Cambridge University Press, Cambridge, United Kingdom and New York, NY, USA.

Camilleri, R., and A. J. Vella (2010), Effect of fireworks on ambient air quality in Malta, *Atmospheric Environment*, **44**, 4521-4527.

Carranza, J.E., B. T. Fisher, G. D. Yoder, and D. W. Hahan (2001), On-line analysis of ambient air aerosols using laser-induced breakdown spectroscopy, *Spectrochim Acta, Part B*, **56**, 851-864.

Chan, C. K., and X. H. Yao (2008), Air pollution in mega cities in China - a review, *Atmospheric Environment*, **42**, 1-42.

Chatterjee, A., C. Sarkar, A. Adak, U. Mukherjee, S. K. Ghosh, and S. Raha (2013), Ambient air quality during Diwali Festival over Kolkata – a mega-city in India, *Aerosol and Air Quality Research*, doi: 10.4209/aaqr.2012.03.0062.

Choi, Y., C. Ho, D. Chen, Y. Noh, and C. Song (2008), Spectral analysis of weekly variation in PM10 mass concentration and meteorological conditions over China, *Atmospheric Environment*, **42**, 655-666.

Crespo, J., E. Yuberro, J. F. Nicolás, F. Lucarelli, S. Nava, M. Chiari, and G. Calzolai (2012), High-time resolution and size-segregated elemental composition in high-intensity pyrotechinc exposures, *Journal of Hazardous Materials*, **241-242**, 82-91.

Dan, L., and A. M. Vogelmann (2006), A climatologically significant aerosol longwave indirect effect in the Arctic, *Nature*, **439**, 453-456, doi:10.1038/nature04449

Dee, D. P., S. M. Uppala, A. J. Simmons, and co-authors (2011), The ERA-Interim reanalysis: configuration and performance of the data assimilation system, *Quarterly Journal of the Royal Meteorological Society*, **137**, 553-597, doi:10.1002/qj.828.

Ding Y. H. (2013), *Climate of China*. Beijing, Science Press, p557 (in Chinese)

Ding, A. J., C. B. Fu, X. Q. Yang, J. N. Sun, T. Petäjä, V.-M. Kerminen, T. Wang, Y. Xie, E. Herrmann, L. F. Zheng, W. Nie, Q. Liu, X. L. Wei, and M. Kulmala (2013), Intense atmospheric pollution modifies weather: a case of mixed biomass burning with fossil fuel combustion pollution in eastern China, *Atmospheric Chemistry and Physics*, **13**, 10545-10554, doi:10.5194/acp-13-10545-2013, 2013.

Drewnick, F., S. S. Hings, J. Curtius, G. Eerdekens, and J. Williams (2006), Measurement of fine particulate and gas-phase species during the New Year's fireworks 2005 in Mainz, Germany, *Atmospheric Environment*, **40**, 4316-4327.

Dufresne, J.-L., C. Gautier, P. Ricchiazzi, and Y. Fouquart (2002), Longwave scattering effects of mineral aerosols, *Journal of the Atmospheric Sciences*, **59**, 1959-1966.

Feng, J. M., Y. L. Wang, Z. G. Ma, and Y. H. Liu (2012), Simulating the regional impacts of urbanization and anthropogenic heat release on climate across China, *Journal of Climate*, **25**,7187-7203.

Feng, J. M., J. Wang, and Z. W. Yan (2014), Impact of anthropogenic heat release on regional climate in three vast urban agglomerations in China. *Advances in Atmospheric Sciences*, **31(2)**, 363-373, doi: 10.1007/s00376-013-3041-z.

Flanner, M. G. (2009), Integrating anthropogenic heat flux with global climate models, *Geophysical Research Letters*, **36**, L02801, doi: 10.1029/2008GL036465.

Gong, D. Y., D. Guo, and C.-H. Ho (2006), Weekend effect in diurnal temperature range in China: Opposite signals between winter and summer, *Journal of Geophysical Research-Atmospheres*, **111**, D18113, doi: 10.1029/2006JD007068.

Gong, D.Y., C.-H. Ho, D. L. Chen, Y. Qian, Y. S. Choi, and J. W. Kim (2007), Weekly cycle of aerosol-meteorology interaction over China, *Journal of Geophysical Research-Atmospheres*, **112**, D22202, doi:10.1029/2007JD008888.

Hakim, G. J., A. Joly, F. Ayrault, S. Malardel (2003), Cyclones. In: *Encyclopedia of Atmospheric Sciences*, Eds. J. R. Holton, J. A. Curry, and J. A. Pyle , Volume Two. Academic Press, pp589-615.

Hansell, R.A., S.-C. Tsay, N. C. Hsu, Q. Ji, S. W. Bell, B. N. Holben, E. J. Welton, T. L. Roush, W. Zhang, J. Huang, Z. Li, and H. Chen (2012), An assessment of the surface longwave direct radiative effect of airborne dust in Zhangye, China, during the Asian Monsoon Years field experiment (2008), *Journal of Geophysical Research-Atmospheres*, **117**, D00K39, doi:10.1029/2011JD017370.

Hansen, J. E., M. Sato, and R. Ruedy (1997), Radiative forcing and climate response, Journal of Geophysical Research-Atmospheres, 102, 6831-6864.

Harrad, S., and L. Laurie (2005), Concentrations, sources and temporal trends in atmospheric polycyclic aromatic hydrocarbon in a major conurbation, *Journal of Environmental Monitoring*, **7**, 722-727.

Huang, Y., R. E. Dickinson, and W. L. Chameides (2006a), Impact of aerosol indirect effect on surface temperature over East Asia, *Proceedings of the National Academy of Sciences of the United States of America*, **103(12)**, 4371-4376.

Huang J, B. Lin, P. Minnis, T. Wang, X. Wang, Y. Hu, Y. Yi, and J. K. Ayers (2006b), Sattellite-based assessment of possible dust aerosols semi-direct effect on cloud water path over East Asia, *Geophysical Research Letters*, **33**, L19802, doi:1029/2006GL026561.

Huang, J., P. Minnis, B. Chen, Z. Huang, Z. Liu, Q. Zhao, Y. Yi, and J. K. Ayers (2008), Long-range transport and vertical structure of Asian dust from CALIPSO and surface measurements during PACDEX, *Journal of Geophysical Research-Atmospheres*, **113**, D23212, doi:10.1029/2008JD010620

Huang, J., Q. Fu, J. Su, Q. Tang, P. Minnis, Y. Hu, Y. Yi, and Q. Zhao (2009), Taklimakan dust aerosol radiative heating derived from CALIPSO observations using the Fu-Liou radiation model with CERES constraints, *Atmospheric Chemistry and Physics* ,**9(12)**, 4011-4021.

Jones, C., N. Mahowald, and C. Luo (2004), Observational evidence of African desert dust intensification of easterly waves, *Geophysical Research Letters*, **31**, L17208, doi:10.1029 /2004GL020107.

Lei, Y., Q. Zhang, K. B. He, and D. G. Streets (2011a), Primary anthropogenic aerosol emission trends for China, 1990-2005, *Atmospheric Chemistry and Physics*, **11**, 931-954, doi: 10.5194/acp-11-931-2011.

Li, W., Z. Shi, C. Yan, L. Yang, C. Dong, and W. Wang (2013), Individual metal-bearing particles in a regional haze caused by firecracker and firework emissions, *Science of the Total Environment*, **443**, 464-469.

Lin, J.-T., and M. B. McElroy (2011), Detection from space of a reduction in anthropogenic emissions of nitrogen oxides during the Chinese economic downturn,*Atmospheric Chemistry and Physics*, **11**, 8171-8188.

Liu, D.Y., D. Rutherford, M. Kinsey, and K. A. Prather (1997), Real-time monitoring of pyrotechnically derived aerosol particles in the troposphere, *Analytical Chemistry*, **69**, 1808-1814.

Lu, Z., D. G. Streets, Q. Zhang, S. Wang, G. R. Carmichael, Y. F. Cheng, C. Wei, M. Chin, T. Diehl, and Q. Tan (2010), Sulfur dioxide emissions in China and sulfur trends in East Asia since 2000, *Atmospheric Chemistry and Physics*, **10**, 6311-6331, doi:10.5194/acp-10-6311-2010.

Lu, Z., Q. Zhang, and D. G. Streets (2011), Sulfur dioxide and primary carbonaceous aerosol emissions in China and India, 1996-2010, *Atmospheric Chemistry and Physics*, **11**, 9839-9864, doi:10.5194/acp-11-9839-2011.

Moreno, T., X. Querol, A. Alastuey, F. Amato, J. Pey, M. Pandolfi, N. Kuenzli, L. Bouso, M. Rivera, and W. Gibbons (2010), Effect of fireworks events on urban background trace metal aerosol concentrations: Is the cocktail worth the show? *Journal of Hazardous Materials*, **183**, 945-949.

Nishanth, T., K. M. Praseed, K. Rathnakaran, M. K. S. Kumar, R. R. Krishna, and K. T. Valsaraj (2012), Atmospheric pollution in a semi-urban, coastal region in India following festival seasons, *Atmospheric Environment*, **47**, 295-306.

Park, T.-W., C.-H. Ho, S.-J. Jeong, Y.-S. Choi, S. K. Park, and C.-K. Song (2011), Different characteristics of cold day and cold surge frequency over East Asia in a global warming situation, *Journal of Geophysical Research-Atmospheres*, **116**, D12118, doi:10.1029/2010JD015369.

Qian, Y., D. P. Kaiser, L. R. Leung, and M. Xu (2006), More frequent cloud-free sky and less surface solar radiation in China from 1955-2000, *Geophysical Research Letters*, **33**, L01812, doi:10.1029/2005GL024586.

Qian, Y., L. R. Leung, S. J. Ghan, and F. Giorgi (2003), Regional climate effects of aerosols over China: Modeling and observation, *Tellus Series B*, **55**, 914-934.

Qu, W. J., R. Arimoto, X. Y. Zhang, C. H. Zhao, Y. Q. Wang, L. F. Sheng, and G. Fu (2010), Spatial distribution and interannual variation of surface PM10 concentrations over eighty-six Chinese cities, *Atmospheric Chemistry and Physics*, **10**, 5641-5662, doi:10.5194/acp-10-5641-2010.

Ravindra, K., S. Mor, and C. P. Kaushik (2003), Short-term variation in air quality associated with firework events: A case study, *Journal of Environmental Monitoring*, **5**, 260-264.

Richter, A., J. P. Burrows, H. Nüb, C. Granier, and U. Niemeier (2005), Increase in tropospheric nitrogen dioxide over China observed from space, *Nature*, **437**, 129-132.

Rienecker, M. M., M. J. Suarez, R. Gelaro, and co-authors (2011), MERRA - NASA's Modern-Era Retrospective Analysis for Research and Applications, *Journal of Climate*, **24(14)**, 3624-3648.

Saikawa, E., J. Kurokawa, M. Takigawa, J. Borken-Kleefeld, D. L. Mauzerall, L. W. Horowitz, and T. Ohara (2011), The impact of China's vehicle emissions on regional air quality in 2000 and 2020: a scenario analysis, *Atmospheric Chemistry and Physics*, **11**, 9465-9484, doi:10.5194/acp-11-9465-2011.

Sanchez-Lorenzo, A., P. Laux, H.-J. Hendricks Franssen, J. Calbó, S. Vogl, A. K. Georgoulias, and J. Quaas (2012), Assessing large-scale weekly cycles in meteorological variables: a review, *Atmospheric Chemistry and Physics*, **12**, 5755-5771, doi:10.5194/acp-12-5755-2012.

Song, C. K., C. H. Ho, R. J. Park, Y. S. Choi, J. H. Kim, D. Y. Gong, and Y. B. Lee (2009), Spatial and seasonal variations of surface PM10 concentration and MODIS aerosol optical depth over China, *Asia-Pacific Journal of Atmospheric Sciences*, **45(1)**, 33-43.

Tan, P.-H., C. Chou, J.-Y. Liang, C. C.-K. Chou, and C.-J. Shiu (2009), Air pollution 'Holiday effect' resulting from the Chinese New Year, *Atmospheric Environment*, **43**, 2114-2124.

Vecchi, R., V. Bernardoni, D. Cricchio, A. D'Alessandro, P. Fermo, F. Lucarelli, S. Nava, A. Piazzalunga, and G. Valli (2008), The impact of fireworks on airborne particles, *Atmospheric Environment*, **42**, 1121-1132.

Wang, K.C., R. E. Dickinson, L. Su, and K. E. Trenberth (2012a), Contrasting trends of mass and optical properties of aerosols over the Northern Hemisphere from 1992 to 2011, *Atmospheric Chemistry and Physics*, **12**, 9387-9398.

Wang, S., D. G. Streets, Q. Zhang, K. He, D. Chen, S. Kang, Z. Lu, and Y. Wang (2010), Satellite detection and model verification of NOx emissions from power plants in Northern China, *Environmental Research Letters*, **5**, 044007, doi:10.1088/1748-9326/5/4/044007.

Wang, W. S., D. Y. Gong, Z. Y. Zhou, and Y. X. Guo (2012b), Robustness of the aerosol weekly cycle over southeastern China, *Atmospheric Environment*, **61**, 409-418.

Wang, Y., G. Zhuang, C. Xu, and Z. An (2007), The air pollution caused by the burning of fireworks during the lantern festival in Beijing, *Atmospheric Environment*, **41**, 417-431.

Wang, Y., M. Wang, R. Zhang, S. J. Ghan, Y. Lin, J. Hu, B. Pan, M. Levy, J. H. Jiang, and M. J. Molina (2014), Assessing the effects of anthropogenic aerosols on Pacific storm track using a multiscale global climate model, *Proceedings of the National Academy of Sciences*, doi: 10.1073/pnas.1403364111.

Wang, Z. Y. and Y. H. Ding (2006), Climate change of the cold wave frequency of China in the last 53 years and the possible reasons, *Chinese Journal of Atmospheric Sciences*, **30(6)**,1068-1076. (in Chinese with English Abstract)

Xin, J. Y., Y. S. Wang, L. L. Wang, G. Q. Tang, Y. Sun, Y. P. Pan, and D. S. Ji (2012), Reductions of PM2.5 in Beijing-Tianjin-Hebei urban agglomerations during the 2008 Olympic Games, *Advances in Atmospheric Sciences*, **29(6)**, 1330-1343.

Yang, W., B. Chen, and X. Cui (2014), High-Resolution Mapping of Anthropogenic Heat in China from 1992 to 2010, *Internationa Journal of Environmental Research and Public Health*, **11**, 4066-4077, doi:10.3390/ijerph110404066.

Zhang, M., X. Wang, J. Chen, T. Cheng, T. Wang, X. Yang, Y. Gong, F. Geng, and C. Chen (2010), Physical characterization of aerosol particles during the Chinese New Year's firework events, *Atmospheric Environment*, **44**, 5191-5198.

Zhang, Q., D. G. Streets, G. R. Carmichael, K. B. He, H. Huo, A. Kannari, Z. Klimont, I. S. Park, S. Reddy, J. S. Fu, D. Chen, L. Duan, Y. Lei, L. T. Wang, and Z. L. Yao (2009), Asian emissions in 2006 for the NASA INTEX-B mission, *Atmospheric Chemistry and Physics*, **9**, 5131-5153.

Zhang, Q., D. G. Streets, K. He, Y. X. Wang, A. Richter, J. P. Burrows, I. Uno, C. J. Jang, D. Chen, Z. Yao, and Y. Lei (2007), NOx emission trends for China, 1995-2004: The view from the ground and the view from space, *Journal of Geophysical Research*, **112**, D22306, doi:10.1029/2007JD008684.

Zhang, R., G. Li, J. Fan, D. L. Wu, and M. J. Molina (2007), Intensification of Pacific storm track linked to Asian pollution, *Proceedings of the National Academy of Sciences*, **104(13)**, 5295-5299.

Zhu, J. L., H. Liao, and J. P. Li (2012), Increases in aerosol concentrations over eastern China due to the decadal-scale weakening of the East Asian summer monsoon, *Geophysical Research Letters*, **39**, L09809, DOI: 10.1029/2012GL051428.

Dao-Yi Gong, State Key Laboratory of Earth Surface Processes and Resource Ecology (ESPRE), Beijing Normal University, Beijing 100875, China (gdy@bnu.edu.cn)

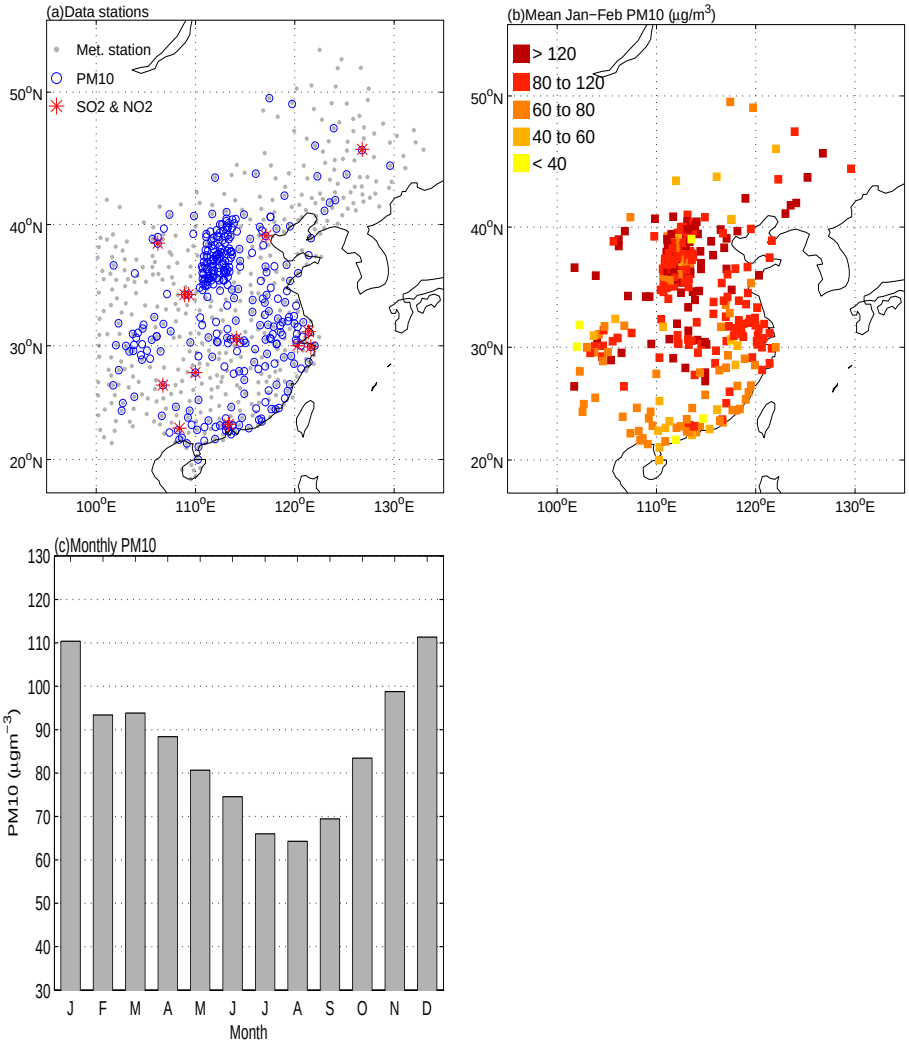

Figure 1. (a) Geographical locations of the 323 PM_{10} stations, 516 meteorological stations, and 13 NO_2 and SO_2 stations. (b) Spatial distribution of January-February averaged PM_{10} concentration. (c) Monthly mean PM_{10} over eastern China.

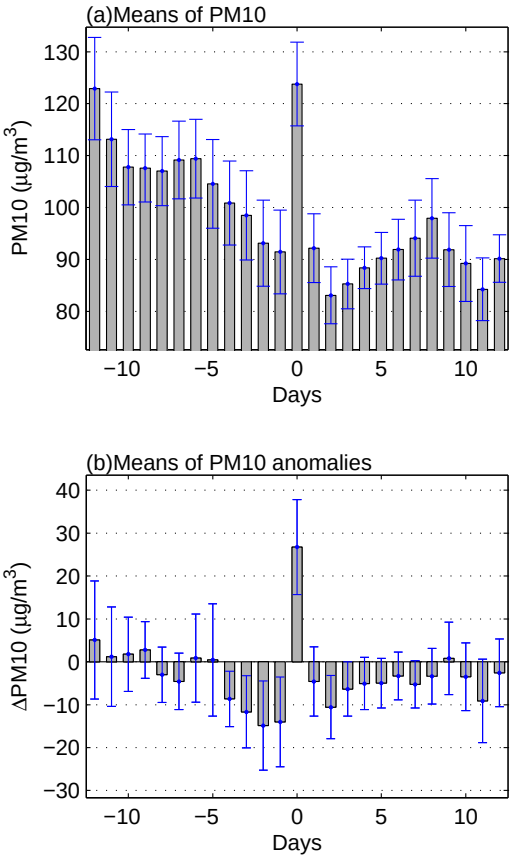

Figure 2. The mean PM_{10} concentration as computed based on all 323 stations (a), and the anomalies of PM_{10} concentration. Day '0' denotes the Chinese New Year day, 10 days before and after the New Year are referred to as days -10 and $+10$ respectively. Only years with >50% station data available are used for anomalous composites. Standard error is shown as error bars.

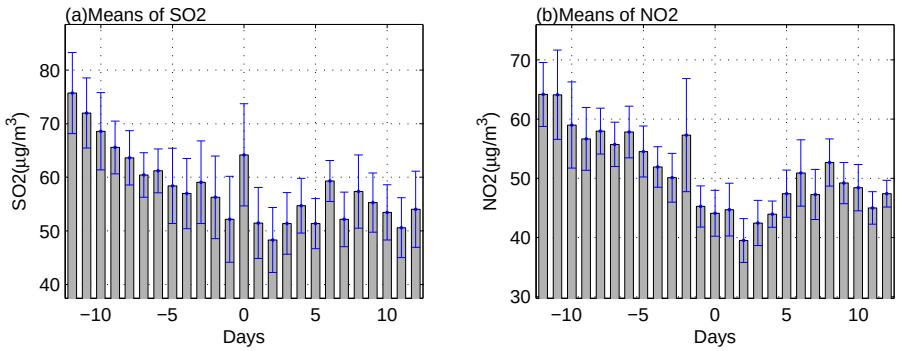

Figure 3. Mean concentrations of SO_2 and NO_2 averaged from 13 stations. See Figure 1 for their locations.

Accepted draft, April 30, 2014

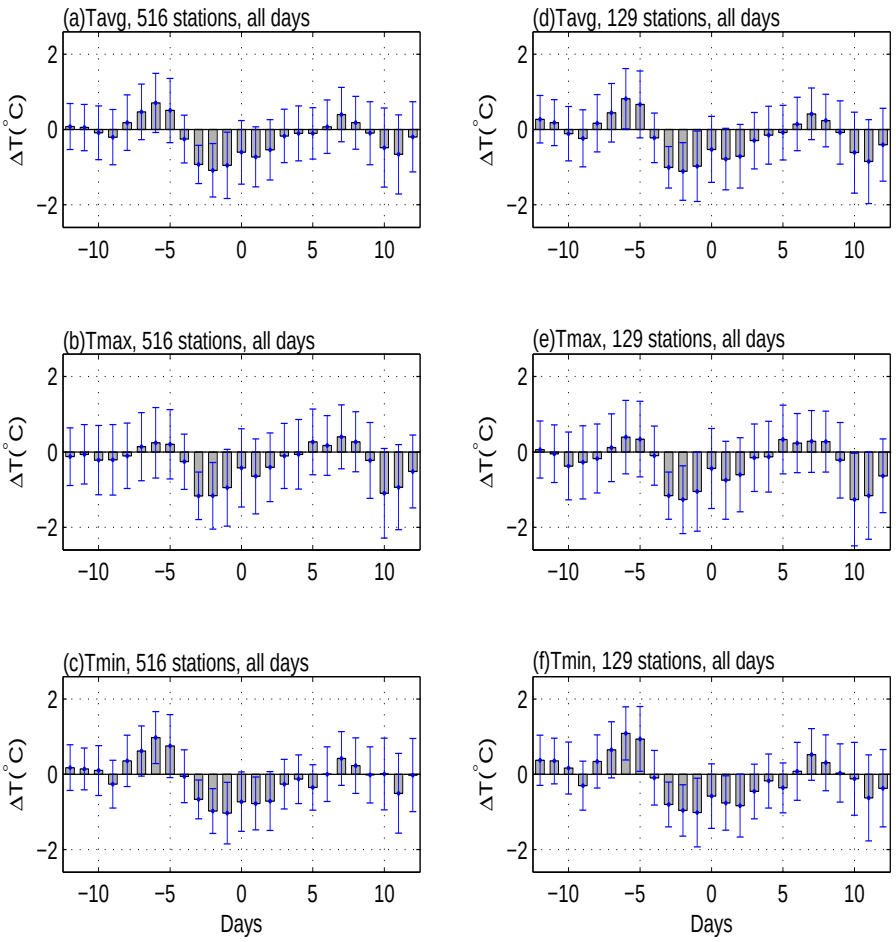

Figure 4. Means of temperature anomalies during the holidays estimated from all available days. Shown in (a, b, c) are temperatures for 516 meteorological stations. Shown in (d, e, f) are temperatures for 129 PM_{10} collocate stations. Tavg, Tmax and Tmin denote the daily mean, daily maximum, and minimum temperature, respectively.

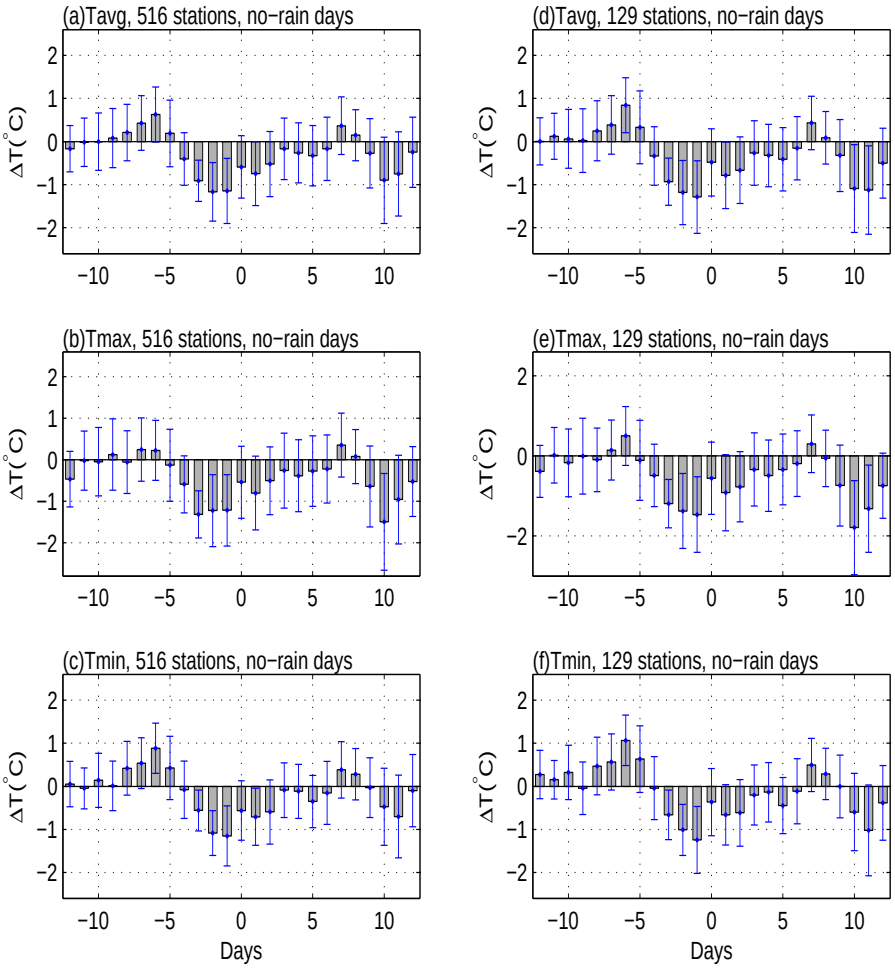

Figure 5. Same as Figure 4, but for the no-rain days.

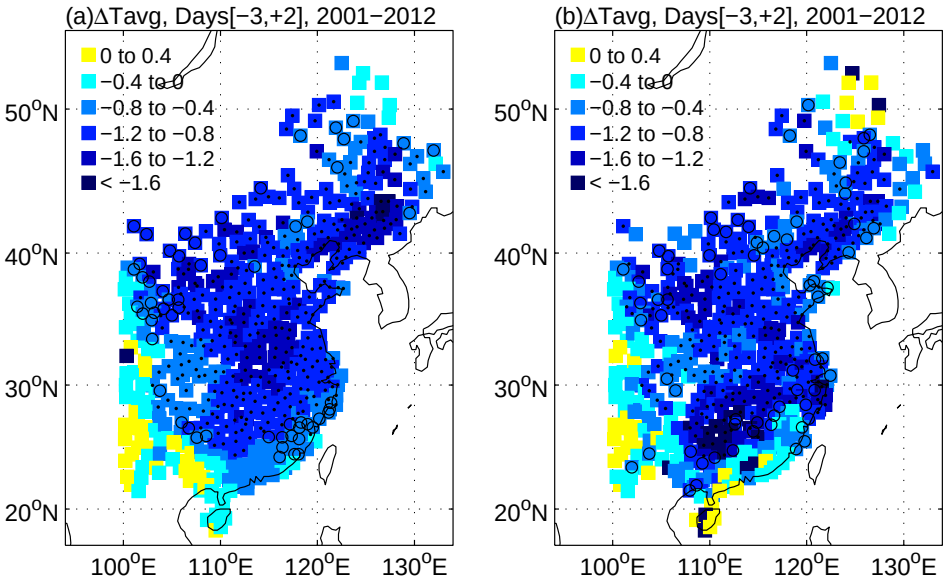

Figure 6. Spatial distribution of mean temperature anomalies averaged from day −3 to day +2 for all available days (a) and for no-rain days (b). The significance level is estimated using a left-tail t-test and values significant above the 0.1 and 0.05 levels are indicated by 'o' and '.', respectively. Units: °C.

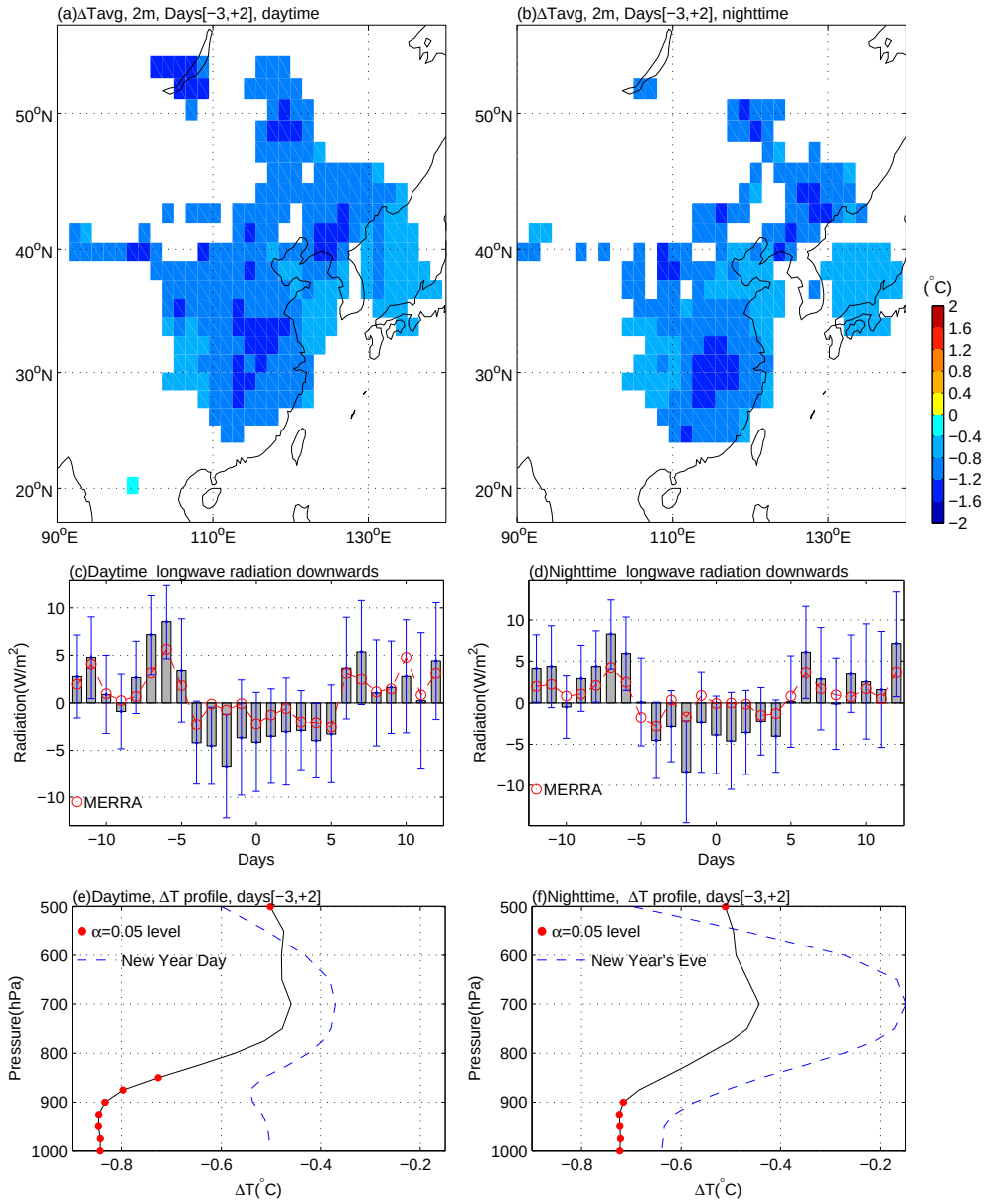

Figure 7. ERA-Interim 2m temperature anomalies averaged from day −3 to day +2 for daytime (a) and nighttime (b). Only temperatures significant above the 0.05 level are plotted. The corresponding anomalies of downward long-wave radiation are shown in (c) and (d). The MERRA longwave flux are plotted together for comparison. The vertical profiles of the temperature anomalies below 500hPa are shown in (e) and (f). The profiles for New Year's Eve and New Year Day are plotted for comparison.

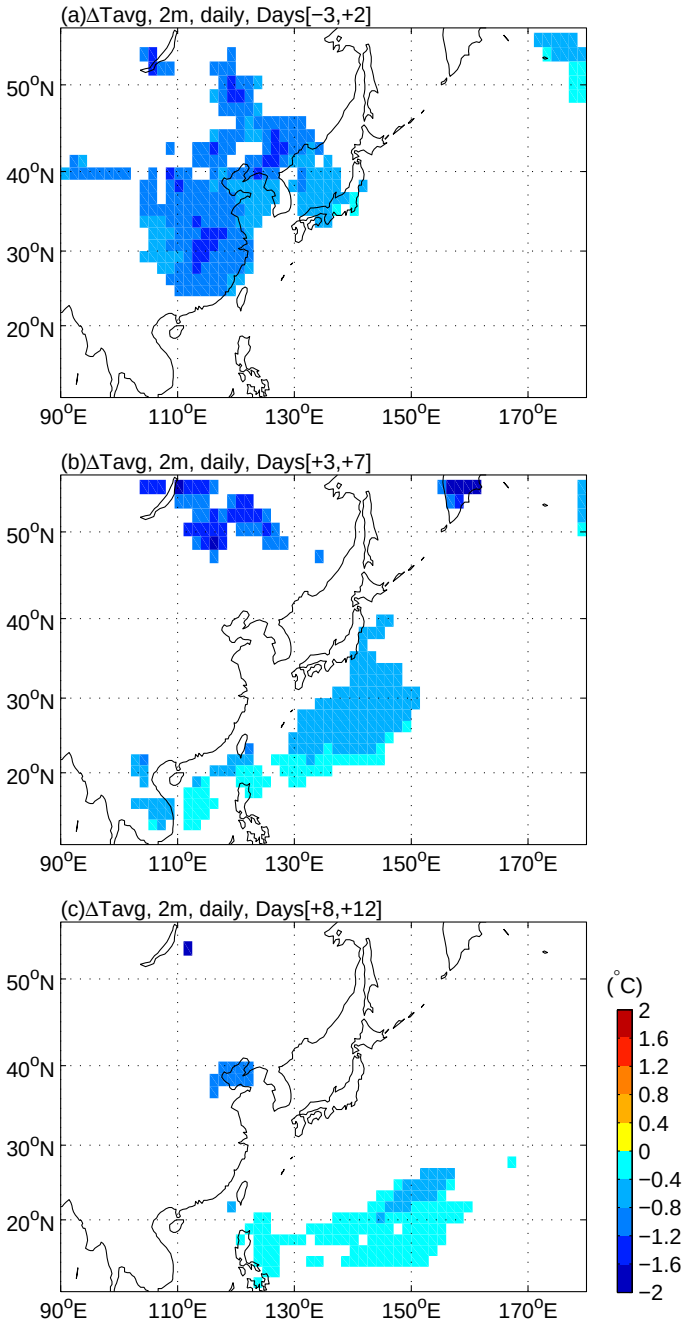

Figure 8. Spatial distribution of ERA-Interim 2m temperature anomalies during different time segments. Only significant values (above the 0.05 level) are plotted.

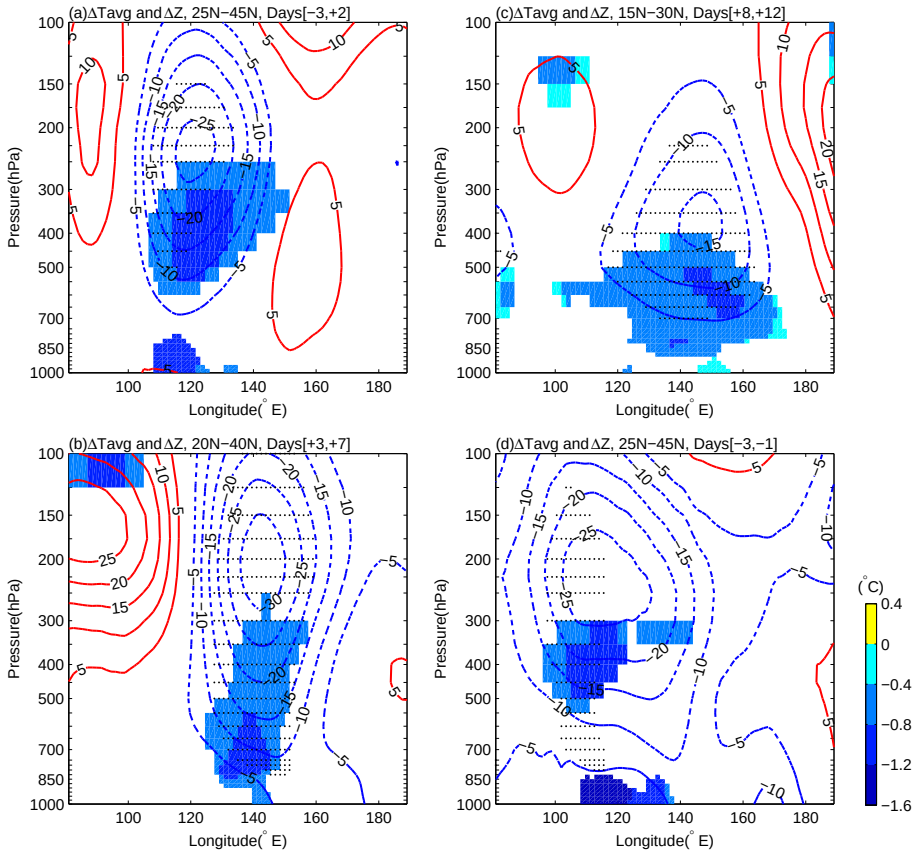

Figure 9. Vertical profile of the air temperature and geopotential height anomalies for different time segments. Significant (at the 0.05 level) temperature anomalies are shown in color shadings. Height anomalies (in meter) are shown as contour lines, blue lines denote negative anomalies and the red denote the positive. The significant heights are indicated by black stipples.

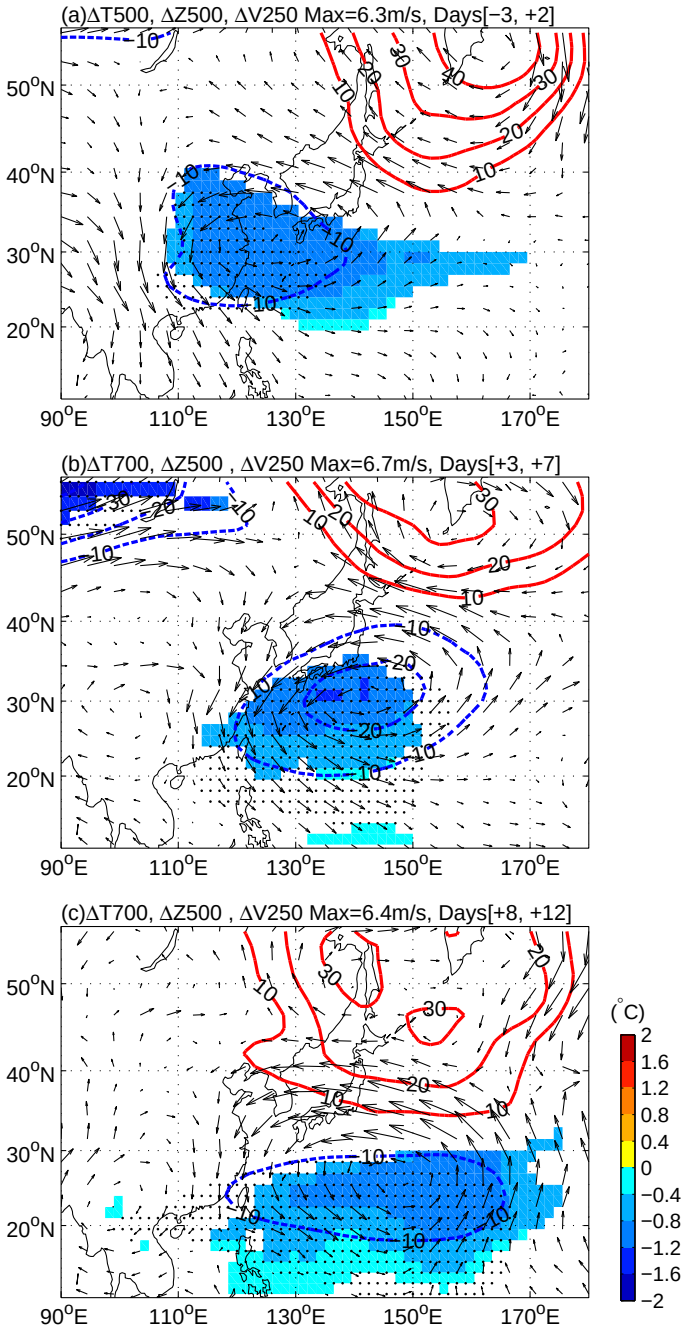

Figure 10. Spatial distribution of the mean anomalies of 500hPa (a) and 700hPa (b, c) temperatures (in color shading), 500hPa geopotential heights (in contour lines with unit of meter, blue lines denote negative anomalies and the red denote the positive), and 250hPa horizontal winds (in vectors with unit of ms^{-1}) during different time segments. Of temperature anomalies only significant (above the 0.05 level) grids are plotted. Significant height anomalies are indicated by black stipples.

Accepted draft, April 30, 2014

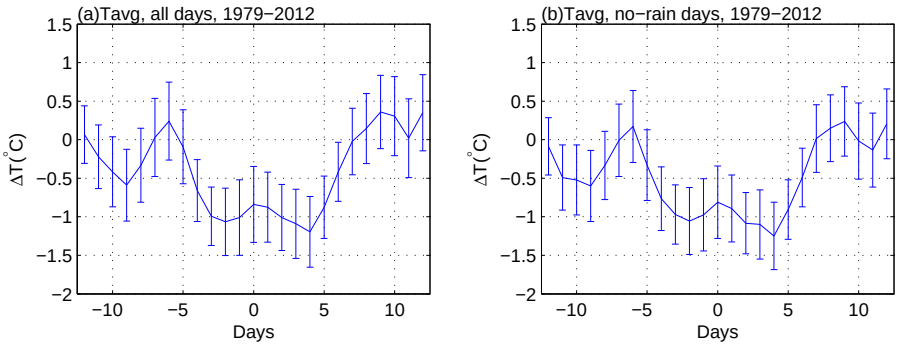

Figure 11. Means of temperature anomalies during the holidays for data period of 1979–2012. (a)As estimated from all available days, and (b) from no-rain days.

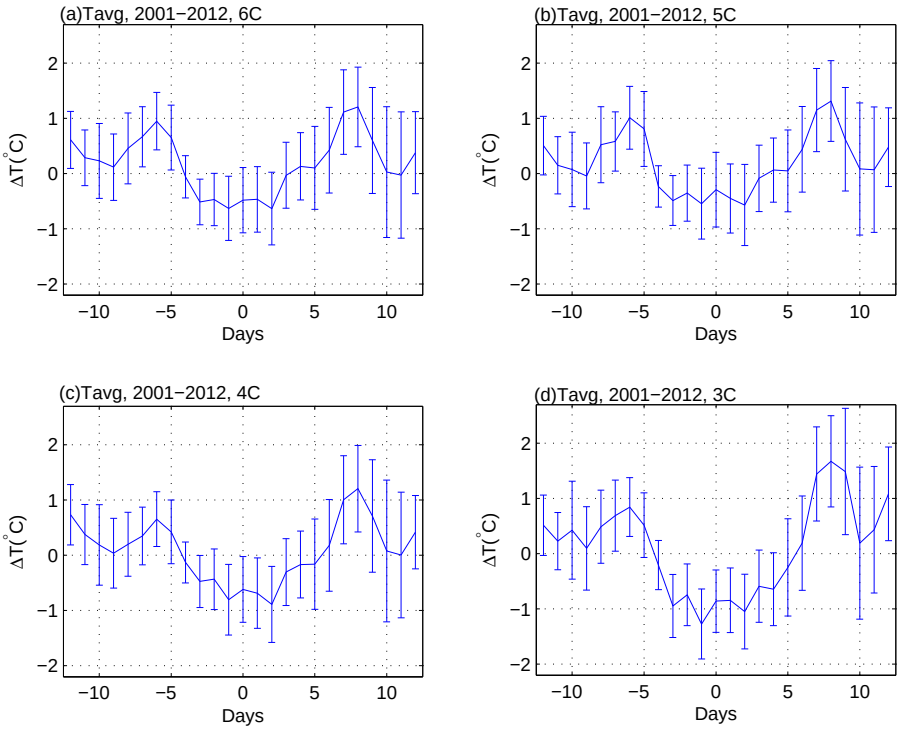

Figure 12. Means of temperature anomalies during the holidays for data period of 2001–2012. Weather disturbances are excluded which is defined as the daily temperature anomaly larger than 5°C or the temperature difference in two consecutive days larger than 6°C(a), 5°C(b), 4°C(c) or 3°C(d), see text for detail.

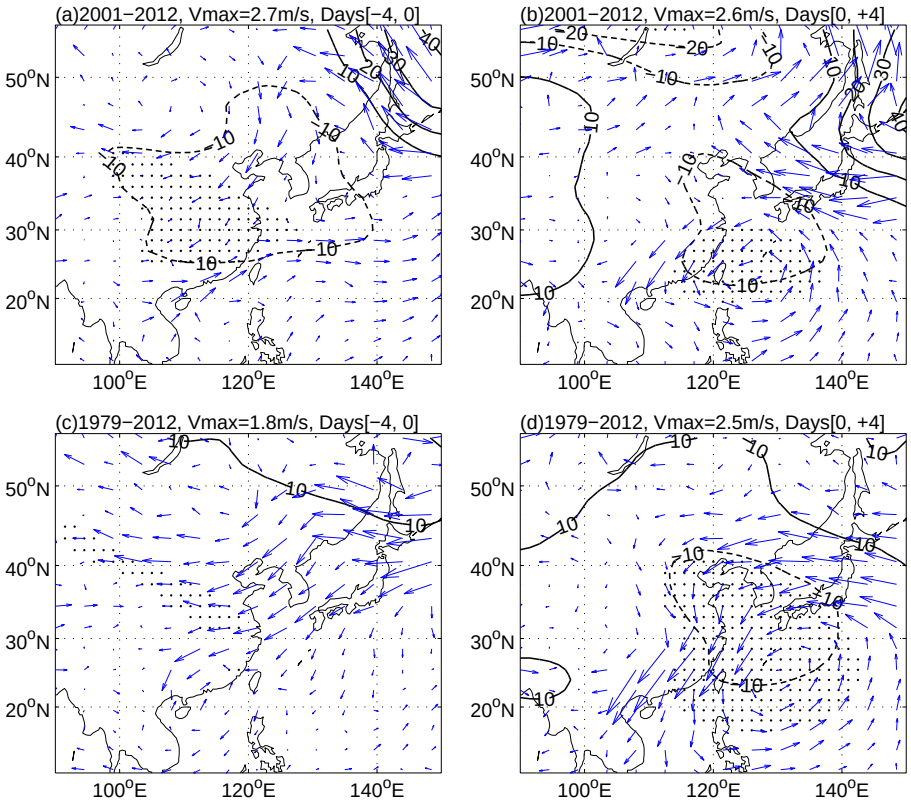

Figure 13. Anomalous 850hPa wind vectors and 500hPa heights in days [−4, 0] and days [0,+4] derived from two data periods of 2001–2012 and 1979–2012. Height anomalies (units: m) are shown as contour lines, solid contours denote the positive anomalies and the dashed contours denote the negative. Height anomalies significant at the 0.05 level are indicated by black stipples.

Table 1. Daily air pollution index sources.

Sources	Station number	Data period
[1]Ministry of Environmental Protection of the People's republic of China	86	2000–2012
[2]Department of Environmental Protection of Shanxi Province	114	2007–2012
[3]Department of Environmental Protection of Guangdong Province	23	2000–2012
[4]Department of Environmental Protection of Liaoning Province	14	2007–2012
[5]Department of Environmental Protection of Hebei Province	12	2002–2012
[6]Department of Environmental Protection of Jiangsu Province	13	2003–2012
[7]Department of Environmental Protection of Hubei Province	17	2002–2012
[8]Department of Environmental Protection of Fujian Province	9	2004–2012
[9]Department of Environmental Protection of Sichuan Province	24	2007–2012
[10]Department of Environmental Protection of Anhui Province	19	2008–2012
[11]Department of Environmental Protection of Jiangxi Province	11	2007–2012
[12]Department of Environmental Protection of Zhejiang Province	11	2004–2012
[13]Department of Environmental Protection of Inner Mongolia Autonomous Region	14	2006–2012
[14]Xinyang City, Luoyang City, Xuchang City of Henan Province	3	2007–2012
[15]Department of Environmental Protection of Guangxi Zhuangzu Autonomous Region	14	2008–2012

[1]www.sepa.gov.cn; [2]www.sxhb.gov.cn; [3]www.gdep.gov.cn; [4]www.lnmc.cn; [5]www.hb12369.net; [6]www.jshb.gov.cn; [7]www.hbepb.gov.cn; [8]www.fjepb.gov.cn;[9]www.scemc.gov.cn; [10]www.aepb.gov.cn; [11]www.jxepb.gov.cn; [12]www.zjepb.gov.cn; [13]www.nmgepb.gov.cn; [14]www.lyhbj.gov.cn; www.xyhbw.gov.cn; www.xchbj.gov.cn; [15]www.gxepb.gov.cn

Table 2. Date of the Chinese New Year from 2001–2012.

Year	Date
2001	24 January
2002	12 February
2003	1 February
2004	22 January
2005	9 February
2006	29 January
2007	18 February
2008	7 February
2009	26 January
2010	14 February
2011	3 February
2012	23 January

Table 3. Statistics for the temperature anomalies during days −3 to +2.

	Means of temperature anomalies (°C)
Station temperature	516 stations (129 stations)
Tavg, all days	−0.81 (−0.85)
Tmax, all days	−0.79[1](−0.88)
Tmin, all days	−0.82(−0.82)
Tavg, no-rain days	−0.85(−0.89)
Tmax, no-rain days	−0.93(−1.05)
Tmin, no-rain days	−0.78(−0.76)
ERA-Interim 2m temperature	
Tavg, daily mean	−0.81
Tavg, daytime	−0.82
Tavg, nighttime	−0.80

[1] significant at the 0.05 level, all others are significant at the 0.01 level.